A Robust Multicopter Control Against Strong Winds

ABSTRACT

The following paper is aimed at achieving a robust multicopter control against external disturbances. Various methodologies have been implemented to achieve disturbance rejection. In an attempt to study the methods and the controllers used to achieve the robust control, a specific situation of wind disturbance will be analysed and results will be demonstrated through simulations. This incorporates the study of different methods used in state estimation through processing of sensor data for robust control.

Key words: Quadrotor, acceleration control, state estimation, robust position control, wind modelling

1 INTRODUCTION

Unmanned Aerial Vehicles have been used quite extensively since the past decade. This includes both fixed wing aircraft as well as multicopters. The use of electric propulsion system increases ease of operation along with low maintenance requirements. Multirotors have, over the years attained agile maneuverability and thus they can be operated in restricted spaces to perform complex missions without human intervention. The requirement for autonomous flight is ever increasing, with added requirements for stability and increased flight times.

The control of a multicopter involves intricate operations to achieve position control and attitude control [4]. A mathematical model involves complex rotations and translation operations while considering the inertial frame and the body fixed frame of reference. Achieving robustness is important since the multirotor is subjected to external disturbances, with wind contributing a significant part as a disturbance [1][2]. In cases where the effects of the wind are strong and pronounced, achieving stability and control against such winds is a daunting task [3].

This provides a motivation to study the concepts behind state estimation which can eliminate unnecessary noise from the sensors.

2 MATHEMATICAL MODEL

The equations of motion of a quadrotor along with some preliminaries are discussed in this section. The control problem is formulated for a planar motion and later extended to a motion in three dimensions.

2.1 Preliminaries

A quadcopter has four rotors, which act as actuators by generating the desired thrust and moments to achieve the required orientation. The plot of force vs angular velocity shows that the relationship between them is approximately quadratic. In mathematical terms $F_i = k_f \omega_i^2$ and $M_i = k_M \omega_i^2$. Here F_i refers to the thrust force produced by each rotor and M_i is the drag moment of each rotor. k_f is the rotor force constant and k_M is the rotor moment constant. The motors need to produce a sufficient torque to overcome the drag moment.

$$\mathbf{F}=\mathbf{F_1}+\mathbf{F_2}+\mathbf{F_3}+\mathbf{F_4}-mg(\hat{\mathbf{zb}}) \quad (1)$$

$$\mathbf{M}=\mathbf{r_1}\mathrm{x}\mathbf{F_1}+\mathbf{r_2}\mathrm{x}\mathbf{F_2}+\mathbf{r_3}\mathrm{x}\mathbf{F_3}+\mathbf{r_4}\mathrm{x}\mathbf{F_4}+\mathbf{M_1}+\mathbf{M_2}+\mathbf{M_3}+\mathbf{M_4} \quad (2)$$

The resultant Force and Moment is given in equation 1 and equation 2 respectively. However, it is important to note that the motor thrust is limited. Thus the motors can only produce a maximum thrust T_{max} and thus a maximum acceleration a_{max}. This has to be considered along with the control laws to determine the input.

2.2 Quadrotor Kinematics

A rigid body displacement is a map from a collection of points in an object, to its physical manifestation in R^3. As time changes, we get a family of maps which characterizes a rigid body motion, which is a continuous set of displacements. Rigid body displacements must satisfy two important properties, they should preserve lengths and cross products.

While considering the mechanics of a quadrotor, the quadrotor is assumed to be in a body fixed frame with the center of gravity as the origin of the frame. Here b_1, b_2, b_3 are the basis vectors. For the inertial frame x, y, z are the mutually orthogonal unit vectors.

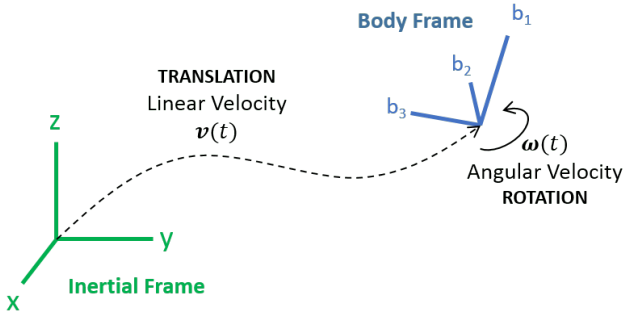

The two frames of reference are shown in figure (2.2) [8], the vectors in a body fixed frame are transformed into vectors in an inertial frame through a *Rotation Matrix*. Euler showed that three coordinates are necessary to specify a rotation, and these are referred to as Euler Angles. Any rotation can be described by three successive rotations about linearly independent axes. A $z-y-x$ rotation can be expressed as rotation about individual axes. This convention produces a rotation matrix R [7].

$$R=Rot(z,\psi)\mathrm{x}Rot(y,\theta)\mathrm{x}Rot(x,\phi) \quad (3)$$

$$R=\begin{bmatrix} c(\theta)c(\psi) & s(\phi)s(\theta)c(\psi)\text{-}c(\phi)s(\psi) & c(\phi)s(\theta)c(\psi)+s(\phi)s(\psi) \\ c(\theta)s(\psi) & s(\phi)s(\theta)s(\psi)+c(\phi)c(\psi) & -s(\phi)c(\psi)+c(\phi)s(\theta)s(\psi) \\ \text{-}s(\theta) & s(\phi)c(\theta) & c(\phi)c(\theta) \end{bmatrix}$$

The pitch angle θ determines the rotation of the quadcopter around the y-axis. Yaw angle ψ determines the rotation around z-axis and the roll angle ϕ determines rotation around x-axis. These $\mathbf{z}-\mathbf{y}-\mathbf{x}$ Euler angles are called as *Tait-Bryan angles*

The linear position of the quadcopter in the inertial frame is defined with $\boldsymbol{\zeta}$. The attitude (The angular position) is defined with the inertial frame with three Euler angles using $\boldsymbol{\eta}$. Vector $\boldsymbol{\kappa}$ contains linear and angular position vectors. In the body fixed frame, the angular velocity components $\boldsymbol{p,q,r}$ are denoted by the matrix $\boldsymbol{\nu}$

$$\zeta=\begin{bmatrix} X \\ Y \\ Z \end{bmatrix} \qquad \eta=\begin{bmatrix} \phi \\ \theta \\ \psi \end{bmatrix} \qquad \kappa=\begin{bmatrix} \zeta \\ \eta \end{bmatrix} \qquad \nu=\begin{bmatrix} p \\ q \\ r \end{bmatrix}$$

Linear Velocity

The translational velocity in body fixed frame is mapped to inertial frame velocity by the rotation matrix.

$$\begin{bmatrix} \dot{X} \\ \dot{Y} \\ \dot{Z} \end{bmatrix} = \begin{bmatrix} c(\theta)c(\psi) & s(\phi)s(\theta)c(\psi)-c(\phi)s(\psi) & c(\phi)s(\theta)c(\psi)+s(\phi)s(\psi) \\ c(\theta)s(\psi) & s(\phi)s(\theta)s(\psi)+c(\phi)c(\psi) & s(\phi)c(\psi)-c(\phi)s(\theta)s(\psi) \\ -s(\theta) & s(\phi)c(\theta) & c(\phi)c(\theta) \end{bmatrix} \begin{bmatrix} \dot{x_b} \\ \dot{y_b} \\ \dot{z_b} \end{bmatrix}$$

Angular Velocity

Consider a frame $\mathcal{A}$ which is moving w.r.t a fixed frame $\mathcal{B}$. The angular velocity $\omega_{\mathcal{AB}}$ describes the rotational motion of $\mathcal{B}$ w.r.t $\mathcal{A}$.

It can be shown that the relationship between angular velocity vector $\omega_{\mathcal{AB}}$ and a time varying rotation matrix $C_{\mathcal{AB}}(t)$ is defined by:

$$[\omega_{\mathcal{AB}}]_x=\dot{C} \cdot C^T_{\mathcal{AB}} \tag{4}$$

With $[\omega_{\mathcal{AB}}]_x$ being the skew symmetric matrix of $\omega_{\mathcal{AB}}$. Given a set of z-y-x Euler angles, what we need is a map from time derivatives of Euler angles and the angular velocity. This matrix can be denoted by **W**. The columns of this matrix are the components of the unit vectors in a fixed frame, around which angular velocities are applied. These are obtained by selecting the columns of a rotation matrix which is generated by successive elementary rotations as given by the Euler angle parametrization. [9]

$$\nu=W\dot{\eta} \qquad where \qquad W = \begin{bmatrix} 0 & -sin(\psi) & cos(\theta)cos(\psi) \\ 0 & cos(\psi) & cos(\theta)sin(\psi) \\ 1 & 0 & -sin(\theta) \end{bmatrix}$$

The inverse mapping is given by:

$$\dot{\eta}=W^{-1}\nu \quad where \quad W^{-1}= \begin{bmatrix} \frac{cos(\psi)sin(\theta)}{cos(\theta)} & \frac{sin(\psi)sin(\theta)}{cos(\theta)} & 1 \\ -sin(\psi) & cos(\psi) & 0 \\ \frac{cos(\psi)}{cos(\theta)} & \frac{sin(\psi)}{cos(\theta)} & 0 \end{bmatrix}$$

However, the inverse is not always possible. If we check *det*(W), we get $-cos(\theta)$. This means mapping becomes singular when $\theta = \pi/2 + k\pi$, $\forall k \in \mathcal{Z}$. The equations for linear velocity in *inertial frame* and angular velocity in *body fixed frame* describe the quadrotor kinematics. [10]

2.3 Quadrotor Dynamics

Newton-Euler Equations

One of the approaches to dynamic modelling is the Newton-Euler method in which forces and torques are balanced. The Newton equation describes translation motion of the center of mass in the *Inertial frame of reference* [11]

$$m\begin{bmatrix} \ddot{X} \\ \ddot{Y} \\ \ddot{Z} \end{bmatrix} = \begin{bmatrix} 0 \\ 0 \\ -mg \end{bmatrix} + R\begin{bmatrix} 0 \\ 0 \\ F_1+F_2+F_3+F_4 \end{bmatrix}$$

On solving, we get:

$$\begin{bmatrix} \ddot{X} \\ \ddot{Y} \\ \ddot{Z} \end{bmatrix} = \begin{bmatrix} \frac{F_T}{m}[\sin(\phi)\sin(\psi)+\cos(\phi)\cos(\psi)\sin(\theta)] \\ -\frac{F_T}{m}[\cos(\psi)\sin(\phi)-\cos(\phi)\sin(\psi)\sin(\theta)] \\ \frac{F_T}{m}[\cos(\phi)\cos(\theta)-g] \end{bmatrix}$$

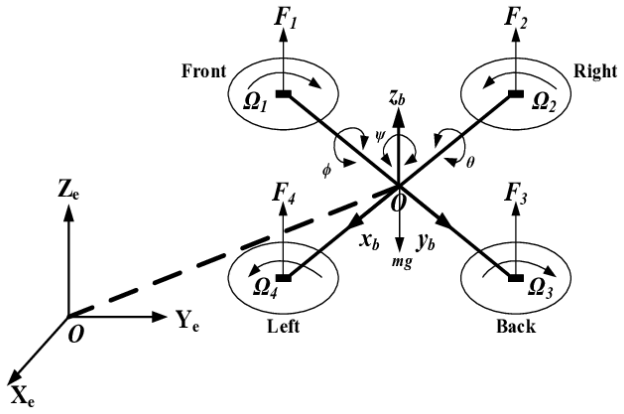

Figure 1. A quadrotor model with body fixed frame and inertial frame [13].

$F_T = F_1+F_2+F_3+F_4$ denotes the total thrust force. R is the rotation matrix to transform vectors in body fixed frame to inertial frame.

The rotational equations of motion are considered in a body fixed frame. This is because the IMU which comprises of the accelerometer, magnetometer and internal gyroscope makes attitude measurements in the body fixed frame. These equations are derived using Euler's equations for rigid body dynamics, which are written as:

$$\mathbf{I}\dot{\omega} + \omega\mathbf{x}(\mathbf{I}\omega) = \mathbf{M_c} \tag{5}$$

Where ω is the angular velocity vector, I is the inertia matrix and M_c is the external torque vector. We consider the symmetry of the quadcopter and model it as two thin uniform rods crossed at the origin, with a motor (point mass) at each end. Based on this assumption, only diagonal elements are non zero.

$$\mathbf{I} = \begin{bmatrix} I_{xx} & 0 & 0 \\ 0 & I_{yy} & 0 \\ 0 & 0 & I_{zz} \end{bmatrix} \qquad \dot{\omega} = \begin{bmatrix} \dot{p} \\ \dot{q} \\ \dot{r} \end{bmatrix} = I^{-1}(M_C - \omega x(I\omega)$$

On substitution and matrix multiplication, we get the following equation. Here the cross product ωxI is written as the skew symmetric cross product matrix $[\omega x]$ pre-multiplying the inertia matrix. The sign convention for elements in this skew symmetric matrix depends on our choice of rotation. ($z-y-x$ in this case).

$$\begin{bmatrix} M_{cx} \\ M_{cy} \\ M_{cz} \end{bmatrix} = \begin{bmatrix} I_{xx} & 0 & 0 \\ 0 & I_{yy} & 0 \\ 0 & 0 & I_{zz} \end{bmatrix} \begin{bmatrix} \dot{p} \\ \dot{q} \\ \dot{r} \end{bmatrix} + \begin{bmatrix} 0 & r & -q \\ -r & 0 & p \\ q & -p & 0 \end{bmatrix} \begin{bmatrix} I_{xx} & 0 & 0 \\ 0 & I_{yy} & 0 \\ 0 & 0 & I_{zz} \end{bmatrix} \begin{bmatrix} p \\ q \\ r \end{bmatrix}$$

$$\begin{bmatrix} \dot{p} \\ \dot{q} \\ \dot{r} \end{bmatrix} = \begin{bmatrix} M_{cx}I_{xx}^{-1} \\ M_{cy}I_{yy}^{-1} \\ M_{cz}I_{zz}^{-1} \end{bmatrix} + \begin{bmatrix} \frac{I_{yy}-I_{zz}}{I_{xx}}qr \\ \frac{I_{zz}-I_{xx}}{I_{yy}}pr \\ \frac{I_{xx}-I_{yy}}{I_{zz}}pq \end{bmatrix} \qquad \begin{bmatrix} M_{cx} \\ M_{cy} \\ M_{cz} \end{bmatrix} = \begin{bmatrix} L(F_3-F_1) \\ L(F_2-F_4) \\ M_2-M_1+M_4-M_3 \end{bmatrix}$$

In the external torque matrix, $F_i = k_f\omega_i^2$ and $M_i = k_M\omega_i^2$. L is the length from the center of mass to end of each arm.

The equations for linear acceleration in *inertial frame* and angular acceleration in *body fixed frame* form the dynamics of the quadrotor. However many effects such as surrounding fluid velocities (Wind), ground effects, blade flapping which lead to highly non-linear dynamics are not considered in this model. [12]

3 WIND MODELLING

Wind speed consists of four components. The first three components- the mean wind speed, the gust wind speed and the ramp wind speed are given analytically. The fourth component- turbulence is the one we are concerned about. Turbulence is caused in the atmosphere by movement of air on small scale due to instabilities in pressure and temperature. Various wind models are used to simulate the effects of turbulence on the UAVs. The Dryden wind model and the Von Karman model are the prominent ones [15]. The Dryden wind model will be used in this research for simulation.

3.1 Dryden Wind Model

The Dryden wind model establishes the correlation function, from which the spectral function is derived. It assumes that the turbulent flow is homogeneous, isotropic and frozen. An isotropic turbulent flow is a class of homogeneous turbulent flow, whose statistics remain invariant under rotation of the coordinate axes as well as for reflection in a plane.

A "frozen" turbulence field model assumes that the small scales in a turbulence are carried past any measuring point with a significant local mean velocity such that the small scales themselves do not have time to change while being swept past the measuring point. [15] For a wide sense stationary (WSS) process x in continuous time, the auto correlation function is given by *Weiner-Khinchin theorem*. It is defined in terms of statistical expected value. Here asterisk (*) denotes the complex conjugate.

$$\mathcal{R}_X(\tau) = E[x(t)^* x(t-\tau)] \tag{6}$$

$\mathcal{R}_X(\tau)$ in general gives an idea of the correlation between two time intervals $t-\tau$ and t for a random process $x(t)$. If the corresponding values at these two timestamps have a higher resemblance, it is considered to have a stronger correlation.

Power Spectral Density

Power spectral density is used to characterize a random process in the frequency domain. The frequency domain is particularly important to identify and analyse the band in which the multicopter model is significantly affected.

For a wide sense stationary process, the power spectral density is defined as the Fourier transform of $\mathcal{R}_X(\tau)$, where $\mathcal{R}_X(\tau)$ is the auto-correlation function.

$$S_X(f) = \mathcal{F}[\mathcal{R}_X(\tau)] = \int_{-\infty}^{\infty} \mathcal{R}_X(\tau) e^{-j2\pi f \tau} d\tau \tag{7}$$

It can be concluded that $\mathcal{R}_X(\tau)$ is the inverse Fourier transform of $S_X(f)$.

$$\mathcal{R}_X(\tau) = \mathcal{F}^{-1}[S_X(f)] = \int_{-\infty}^{\infty} S_X(f) e^{j2\pi f \tau} df \tag{8}$$

$S_X(f)$ is even, non negative and real valued in f. It is usually desirable to have turbulence velocities as a function of time. However, a spatially referenced spectra is of interest for turbulence modelling. Exact filters can be designed that take white noise inputs and output stochastic processes which have the power spectral densities of the Dryden gusts. The power spectral densities are specified for linear as well as angular velocity components of continuous gusts. These power spectral densities are derived experimentally and comply with the MIL-F-8785C military specifications.

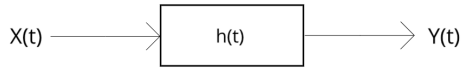

3.2 Linear Time Invariant Systems

The LTI system is used with the aim to design a linear time-invariant filter that takes in Gaussian white noise as input and outputs a turbulence signal with a similar frequency spectrum as Dryden power spectral density. An LTI system can be represented by **??**

For a wide-sense stationary process $X(t)$ which is an input, the output $Y(t)$ is also WSS. An LTI system can be completely described by the impulse response.

$$h(t) = T[\delta(t)]$$

The input-output relation is obtained through convolution. In the frequency domain, the system transfer function is the Fourier transform of $h(t)$

$$Y(t) = h(t) * X(t) = \int_{-\infty}^{\infty} h(t) X(t-\alpha) d\alpha$$

$$H(f) = \mathcal{F}[h(t)] = \int_{-\infty}^{\infty} h(t) e^{-j2\pi f t} dt$$

It can be shown that X(t) and Y(t) are jointly WSS processes. The mean function of $Y(t)$, $\mu_Y(t)$ is given as

$$\mu_Y(t) = E[Y(t)] = E\left[\int_{-\infty}^{\infty} h(\alpha) X(t-\alpha) d\alpha\right] = \int_{-\infty}^{\infty} h(\alpha) E[X(t-\alpha)] d\alpha$$

$$\mu_Y(t) = E[Y(t)] = \int_{-\infty}^{\infty} \mu_X h(\alpha) d\alpha = \mu_X \int_{-\infty}^{\infty} h(\alpha) d\alpha$$

The above equation states that μ_Y is not a function of t. The cross correlation function, $R_{XY}(t_1, t_2)$ can be found the following way

$$R_{XY}(t_1, t_2) = E[X(t_1), Y(t_2)] = E\left[X(t_1) \int_{-\infty}^{\infty} h(\alpha) X(t_2-\alpha) d\alpha\right]$$

$$E\left[\int_{-\infty}^{\infty} h(\alpha) X(t_1) X(t_2-\alpha) d\alpha\right] = \int_{-\infty}^{\infty} h(\alpha) E\left[X(t_1) X(t_2-\alpha) d\alpha\right]$$

$$\int_{-\infty}^{\infty} h(\alpha) R_x(t_1, t_2-\alpha) d\alpha = \int_{-\infty}^{\infty} h(\alpha) R_x(t_1 - t_2 + \alpha) d\alpha$$

$R_{XY}(t_1, t_2)$ is only a function of $\tau = t_1 - t_2$. Substitution yields:

$$R_{XY}(\tau) = \int_{\infty}^{\infty} h(\alpha) R_x(\tau + \alpha) d\alpha$$
$$= h(\tau) * R_X(-\tau) = h(-\tau) * R_X(\tau)$$

It can be shown similarly that $R_Y(\tau)$ and $R_X(\tau)$ are related by

$$R_Y(\tau) = h(\tau) * h(-\tau) * R_X(\tau)$$

Finally by taking the Fourier transform from both sides, the relation between power spectral densities and the transfer function for a joint WSS processes can be found

$$S_Y(f) = S_X(f) |H(f)|^2$$

Thus, for a given power spectral density for the Dryden model, the transfer function can be found accordingly that acts as a filter on a Gaussian white noise, giving the required turbulence signal.

From the MIL-F-8785C military specifications, the following Dryden power spectral densities are procured [16]

	Power Spectral Density
Longitudinal	
$\phi_u(\omega)$	$\frac{2\sigma_u^2 L_u}{\pi V} \frac{1}{1+\left(L_u \frac{\omega}{V}\right)^2}$
$\phi_p(\omega)$	$\frac{\sigma_w^2}{V L_w} \frac{0.8\left(\frac{\pi L_w}{4b}\right)^{\frac{1}{3}}}{1+\left(\frac{4b\omega}{\pi V}\right)}$
Lateral	
$\phi_v(\omega)$	$\frac{\sigma_u^2 L_v}{\pi V} \frac{1+3\left(L_v \frac{\omega}{V}\right)^2}{\left[1+\left(L_v \frac{\omega}{V}\right)^2\right]^2}$
$\phi_r(\omega)$	$\frac{\pm\left(\frac{\omega}{V}\right)^2}{1+\left(\frac{3b\omega}{\pi V}\right)^2} \cdot \phi_v(\omega)$
Vertical	
$\phi_w(\omega)$	$\frac{\sigma_w^2 L_w}{\pi V} \frac{1+3\left(L_w \frac{\omega}{V}\right)^2}{\left[1+\left(L_w \frac{\omega}{V}\right)^2\right]^2}$
$\phi_q(\omega)$	$\frac{\pm\left(\frac{\omega}{V}\right)^2}{1+\left(\frac{4b\omega}{\pi V}\right)^2} \cdot \phi_w(\omega)$

ω	Temporal frequency
b	Aircraft Wingspan
u,v,w	Disturbance velocity along the x,y,z axes
p,q,r	Disturbance angular velocity about the x,y,z axes
$\sigma_u, \sigma_v, \sigma_w$	Standard deviations of u,v,w
L_u, L_v, L_w	Scale lengths for power spectra

Continuous Dryden Filters

As described in 3.2, the filters can be derived from the spectral square roots of the Dryden spectrum equations. The filters generate a turbulence signal that has a similar frequency spectrum as Dryden power spectral density. The combination of the length scale and turbulence intensity determines the shape of the power spectral densities and thus a realistic fit to observed turbulence.

Gaussian White Noise

Gaussian white noise is a stationary and ergodic random process zero mean that is defined by the following fundamental property: any two values of GWN are statistically independent now matter how close they are in time. For a Gaussian white noise process w(t), the autocorrelation function ϕ_w is zero for non-zero arguments.

$$\phi_w(\tau) = E[w(t)w(t-\tau)] = E[w(t)]E[w(t-\tau)] = 0 \quad \forall \tau \neq 0$$

This means that the variance of the zero mean process is defined as the value of ϕ_w $\tau = 0$. Consequently it should be infinite mathematically. The autocorrelation function can be defined as $\phi_w(\tau) = P\delta(\tau)$. The Fourier transform gives the power spectral density and it is evident that it is constant over all frequencies and is given as $S_w(\omega) = P$

	Dryden Filters
Longitudinal	
$H_u(s)$	$\sigma_u \sqrt{\frac{2L_u}{\pi V}} \frac{1}{1+\left(\frac{L_u}{V}s\right)}$
$H_p(s)$	$\sigma_w \sqrt{\frac{0.8}{V}} \frac{\left(\frac{\pi}{4b}\right)^{\frac{1}{6}}}{L_w^{\frac{1}{3}}\left(1+\left(\frac{4b}{\pi V}\right)s\right)}$
Lateral	
$H_v(s)$	$\sigma_v \sqrt{\frac{L_v}{\pi V}} \frac{1+\frac{\sqrt{3}L_v}{V}s}{\left[1+\left(\frac{L_v}{V}s\right)\right]^2}$
$H_r(s)$	$\frac{\pm\left(\frac{s}{V}\right)}{1+\left(\frac{3b}{\pi V}s\right)} \cdot H_v(s)$
Vertical	
$H_w(s)$	$\sigma_w \sqrt{\frac{L_w}{\pi V}} \frac{1+\frac{\sqrt{3}L_w}{V}s}{\left[1+\left(\frac{L_w}{V}s\right)\right]^2}$
$H_q(s)$	$\frac{\pm\left(\frac{s}{V}\right)}{1+\left(\frac{4b}{\pi V}s\right)} \cdot H_w(s)$

Low Altitude Model

For an altitude of less than or equal to 1000ft, the turbulence scale length, turbulence intensity and turbulence axes orientation are defined. The turbulence scale length is a function of altitude.

$$2L_w = h$$
$$L_u = 2L_v = \frac{h}{(0.177+0.000823h)^{1.2}}$$

Turbulence intensities for the above model are defined as:

$$\sigma_w = 0.1 W_{20}$$

$$\sigma_u = \sigma_v = \sigma_w \frac{1}{(0.177 + 0.000823h)^{0.4}}$$

Where W_{20} represents wind speed values at a height of 20 feet. For different turbulence levels, W_{20} is defined in the following table:

Turbulence Level	W_{20}
Light	15 knots
Moderate	30 knots
Severe	45 knots

4 CONTROLLER DESIGN

A controller is a key aspect of any dynamic system that is intended to follow a reference command. Sensor measurements are used to calculate the errors from desired values. This is used as a feedback mechanism to achieve the desired command (setpoint).

Different control algorithms are used in quadrotor controllers. Some of these include a PID controller [17], Active Disturbance Rejection Controller, Sliding Mode Control (SMC) and Model Predictive Controller (MPC). A PID controller has been used in the implementation of this paper. This section begins with an introduction to the PID controller. The control strategy has been discussed for the quadrotor which consists of an attitude controller and a position controller. Finally some aspects of state estimation also have been discussed which includes the concept of a complimentary filter by Mahony.

PID Controller Design

PID controllers have been used for plants which can incorporate small time delays. Quadrotors are high performance aerial robots that run attitude control loops at approximately 1 kHz. Position control loop controls the three dimensional trajectory of the quadrotor and generally runs at around 100 Hz. [19]

One of the most important forms of the PID controller can be represented as:

$$u(t) = K_p \left[e(t) + \frac{1}{T_i} \int_0^t e(\tau) d\tau + T_d \frac{de(t)}{dt} \right] \tag{9}$$

Here u(t) is the input signal to the quadrotor plant model. e(t) is the error signal. It can be written as:

$$e(t) = r(t) - y(t) \tag{10}$$

Here r(t) is the reference signal and y(t) is the output signal. A PID controller is widely used due to its simplicity and robustness. The gains of the controller can be easily adjusted and configured intuitively. Some of the complexities of a quadrotor include the non-linear mathematical model and dynamics. Application of a PID controller is thus dependant on the need of the user. Non linear controllers can be used for more complex applications. The different parameters that need to be controlled in a quadrotor include altitude, roll angle, pitch angle and yaw rate. The feedback of these parameters from the plant model forms a closed feedback loop.

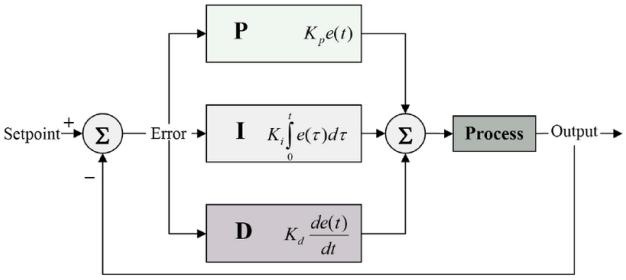

Figure 2. A PID controller within a closed loop control system [22]

A typical PID controller can be represented by figure 2. Since the mathematical model of a quadrotor is not linear, the motor models and equations of motion are linearized at the nominal hover configuration. This is chosen as the operating point for the quadrotor.
For the hover configuration, the following parameters are defined:

$$\begin{array}{lll} \theta = 0 & \phi = 0 & \psi = \psi_o \\ \dot{\theta} = 0 & \dot{\phi} = 0 & \dot{\psi} = 0 \\ c\phi \approx 1 & c\theta \approx 1 & s\phi \approx \phi \\ s\theta \approx \theta & \mathbf{u_{1,0}} = mg & \mathbf{u_{2,0}} = 0 \end{array}$$

Linearizing the Newton- Euler equations with respect to hover state:

$$\begin{aligned} \ddot{X} &= g(\Delta\theta \cos\psi_o + \Delta\phi \sin\psi_o) \\ \ddot{Y} &= g(\Delta\theta \sin\psi_o - \Delta\phi \cos\psi_o) \\ \ddot{Z} &= \frac{\mathbf{u_1}}{m} - g \end{aligned} \tag{11}$$

$$I \begin{bmatrix} \dot{p} \\ \dot{q} \\ \dot{r} \end{bmatrix} = \begin{bmatrix} 0 & L & 0 & -L \\ -L & 0 & L & 0 \\ \gamma & -\gamma & \gamma & -\gamma \end{bmatrix} \begin{bmatrix} F_1 \\ F_2 \\ F_3 \\ F_4 \end{bmatrix} - \begin{bmatrix} p \\ q \\ r \end{bmatrix} \times I \begin{bmatrix} p \\ q \\ r \end{bmatrix}$$

The above equation in hover state gets simplified to equation 4. Here $\gamma = \frac{K_M}{K_F}$

$$\begin{bmatrix} \dot{p} \\ \dot{q} \\ \dot{r} \end{bmatrix} = I^{-1} \begin{bmatrix} 0 & L & 0 & -L \\ -L & 0 & L & 0 \\ \gamma & -\gamma & \gamma & -\gamma \end{bmatrix} \begin{bmatrix} F_1 \\ F_2 \\ F_3 \\ F_4 \end{bmatrix}$$

Position and Attitude Control

From the decoupled equations of motion it can be concluded that rotation and translational motions are independant of each other. While rotational movements are fully actuated, translational movements are dependant on rotation and are thus under actuated. The quadrotor controller thus consists of two feedback loops. The inner loop controls attitude and uses accelerometer and gyroscope measurement to control roll, pitch and yaw. The outer loop is used to control position and trajectory tracking in a three dimensional environment.

A control strategy thus has been developed which uses a PID controller for attitude control. In the next sections, the attitude controller and position controller have been explained, along with the control algorithm for hovering.

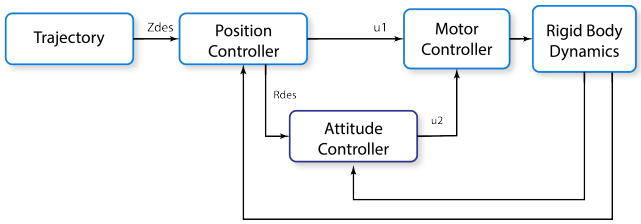

Figure 3. A Quadrotor controller with an attitude and a position control loop

Attitude and Position Control for Hover State

A PID control algorithm is used for trajectory tracking in SO(3) for roll and pitch angles. A PD controller is used for yaw angle. A PD controller is used to calculate the commanded accelerations by driving the error in position to zero. This is represented as:

$$(\ddot{r}_{i,T} - \ddot{r}_{i,des}) + K_d(\dot{r}_{i,T} - \dot{r}_i) + K_p(r_{i,T} - r_i) = 0 \tag{12}$$

The XY positions are used to estimate the desired Pitch and Roll angles. From equation 11, we can write:

$$\begin{aligned} \ddot{X} &= g(\theta_{des}\cos\psi + \phi_{des}\sin\psi) \\ \ddot{Y} &= g(\theta_{des}\sin\psi - \phi_{des}\cos\psi) \\ \ddot{Z} &= \frac{\mathbf{u_1}}{m} - g \end{aligned} \tag{13}$$

The first two equations can be re-written to calculate the desired roll and pitch angles for the controller reference.

$$\begin{aligned} \phi_{des} &= \frac{1}{g}(\ddot{X}\sin\psi - \ddot{Y}\cos\psi) \\ \theta_{des} &= \frac{1}{g}(\ddot{X}\cos\psi + \ddot{Y}\sin\psi) \end{aligned} \tag{14}$$

For the implementation of the PID controller, the desired roll and pitch rates are taken as zero. Figure 4 shows the simulink block, with implementation of the attitude controller.

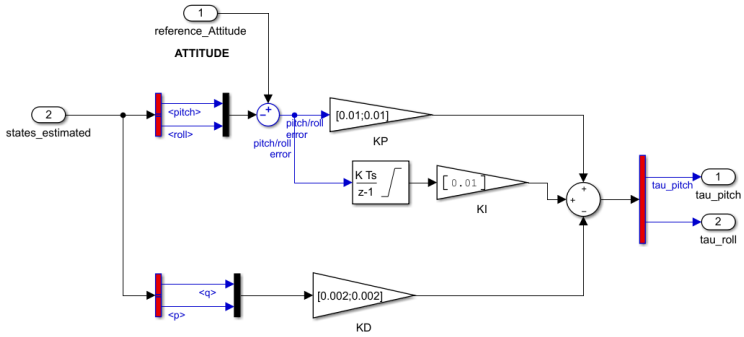

Figure 4: Attitude Controller for Pitch and Roll

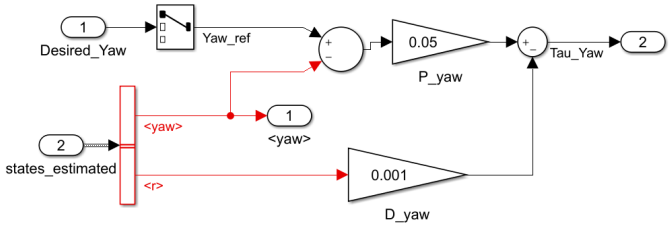

Figure 5: PD Controller for Yaw

	Payload Weight	Cost	Accuracy
GPS	Low	Low	Low
Cameras	Low	Moderate	High
LIDAR	High	High	High

Table 1. Different sensors facilitating state estimation

5 STATE ESTIMATION

Quadrotors primarily deal with states like position, velocity and orientation with reference to an inertial frame. With limited resources and computational power, state estimation becomes a challenging task with the controller loops running at 100 Hz to 1 kHz. In this section, a brief comparison is shown for different sensors used in estimation. Further, a complementary filter is explained along with the algorithm for quaternion based attitude estimation.

Miniature aerial vehicles use an Inertial Measurement Unit (IMU) which comprises of a gyroscope and an accelerometer (3D) to measure linear accelerations and rotational velocities. In principle, these measurements can be integrated to obtain rough estimates of the velocities and position. However, this estimate is highly biased by noise and IMU imperfections. Table 1 shows the types of sensors prominently used for estimation.

Sensor Fusion

Aerial robots sometimes have multiple sensors that measure similar parameters. This facilitates quality improvement in state estimation by fusing the data from both the sensors. It also makes the system robust against sensor failures. Kalman filters have been widely used due to ease of implementation and remarkable performance.

Measurement Models

As discussed in previous subsections, a gyroscope measurement has noise and a bias which varies with time as additional components to the primary measurement of angular velocity. The model can be represented by:

$$\chi_{\omega,t} = \omega^b_{ib,t} + \delta^b_{\omega,t} + e^b_{\omega,t} \tag{15}$$

Here $\omega^b_{ib,t}$ is the angular velocity in body fixed frame at time t. The bias is represented by $\delta^b_{\omega,t}$ and $e^b_{\omega,t}$ is the noise. A similar model can be defined for acceleration measurements and can be stated as:

$$\chi_{a,t} = f^b_t + \delta^b_{a,t} + e^b_{a,t} \tag{16}$$

The accelerometer noise has a distribution similar to that of a Gaussian curve.

Complementary Filter

Gyroscopes tend to have accurate measurements with little noise. However, since the angular rates have to be integrated, the error also adds up which results in a net drift. Accelerometer is sensitive to any external disturbances. A complimentary filter is thus used to fuse the estimates from both sensors to overcome the drawbacks of each sensor. Since it is impossible for yaw angle estimation directly, the drift is neglected and values are inferred from accelerometer and gyroscope. [18]

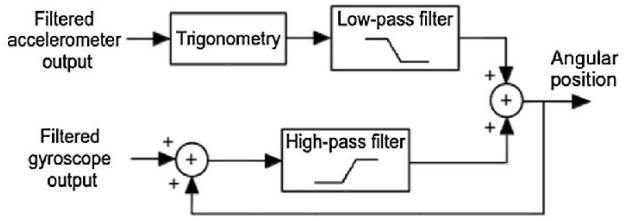

Figure 6. Complementary Filter [20]

Accelerometer Estimation

The raw data from accelerometer is used to estimate roll and pitc angles. They are found using the following set of equations

$$\phi_{acc} = arctan\left(\frac{a_y}{a_z}\right)$$

$$\theta_{acc} = arctan\left(\frac{-a_x}{\sqrt{a_y^2 + a_z^2}}\right) \quad (17$$

Mahony Filter

Mahony filter [23] is quite popular for the relatively faster computation speeds. It can be tuned by $K_{p-mahony}$ & $K_{i-mahony}$. The algorithm of Mahony filter is discussed below. [24]

Algorithm Steps

Normalize acceleration vector

$$\vec{a_k} = [a_{x,k} \quad a_{y,k} \quad a_{z,k}]$$

$$\vec{a_k} = \frac{\vec{a_k}}{||\vec{a_k}||}$$

Estimate direction of gravity field

$$\hat{q_{k-1}} = [q_1 \quad q_2 \quad q_3 \quad q_4]$$

$$v = \begin{bmatrix} 2(q_2q_4 - q_1q_3) \\ 2(q_1q_2 + q_3q_4) \\ q_1^2 - q_2^2 - q_3^2 + q_4^2 \end{bmatrix}$$

Error is the cross product between acceleration vector and gravity field

$$e = \vec{a_k} \times v$$

$$E_k = E_{k-1} + e_{\Delta t}$$

Modify the angular rate vector

$$\vec{\omega_k} = \vec{\omega_{k-1}} + K_{p,mahony}e + K_{i,mahony}E_k$$

Calculate the rate of change of attitude quaternion

$$\dot{q} = \frac{1}{2}\hat{q}_{k-1} \times \vec{\omega_k} = \frac{1}{2}[q_1 \quad q_2 \quad q_3 \quad q_4] \times [0 \quad \omega_{x,k} \quad \omega_{y,k} \quad \omega_{z,k}]$$

Quaternion Normalization

$$\hat{q}_k = \hat{q}_{k-1} + \dot{q}\Delta t$$

$$\hat{q_k} = \frac{\hat{q_k}}{||\hat{q_k}||}$$

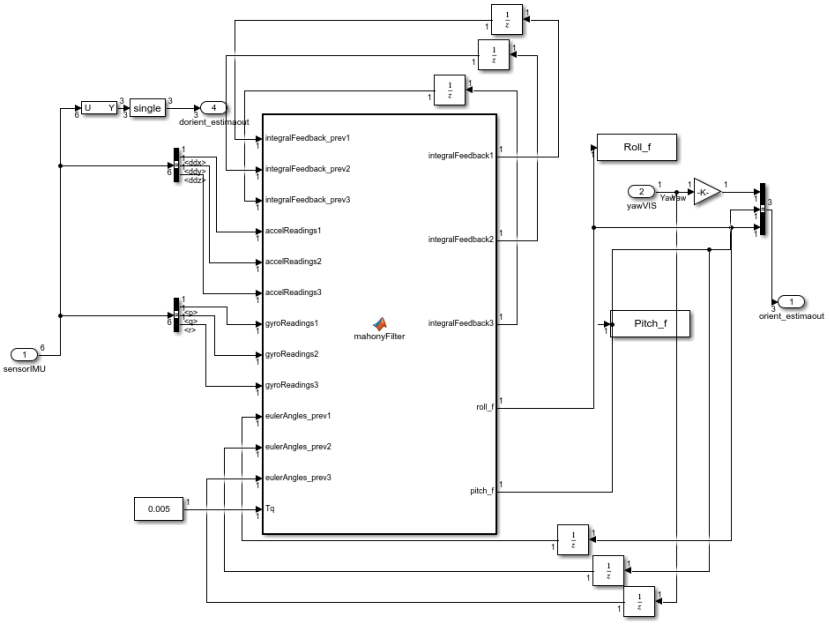

Figure 7: Mahony Filter

Figure 7 shows the implementation of Mahony Filter in Simulink.

The filter takes in sample time as an input and performs integration in steps accordingly for discrete time values.

6 CONCLUSION AND FUTURE WORK

This work was initially aimed towards achieving a robust multirotor control against strong winds. In the duration of the entire project, significant progress has been made towards the study of wind modelling and controller approach. However, wind estimation and incorporation of the feedback to counter the acceleration due to wind is yet to be implemented on the controller. This needs to be implemented and the results should be studied. The work presented here provides an approach to the said problem statement.

7 ACKNOWLEDGEMENT

I have been grateful to Prof. Hemendra Arya for the guidance and intellectually stimulating conversations throughout the duration of the project. I have been able to learn a lot and would continue my work and exploration in the domain of Aerial Robotics.

APPENDIX A: SIMULATION GRAPHS

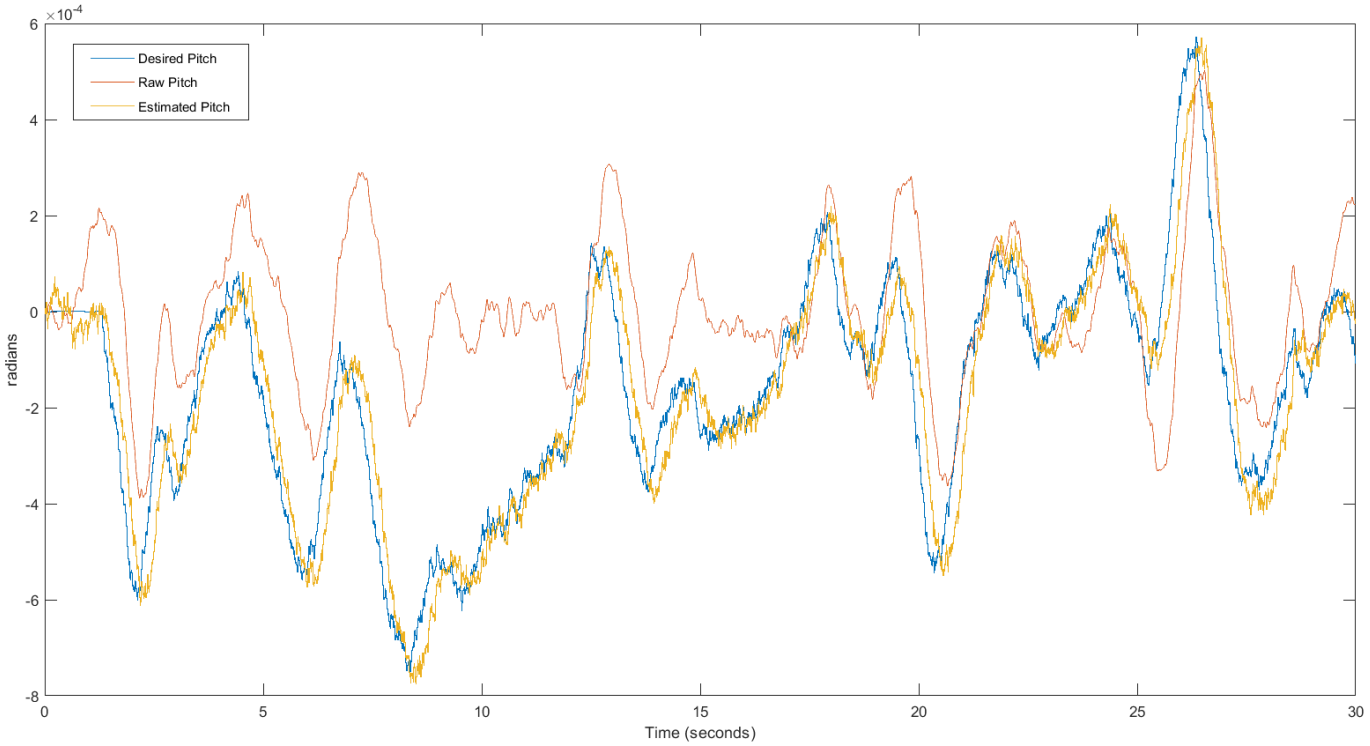

Figure A1: Pitch data at hover

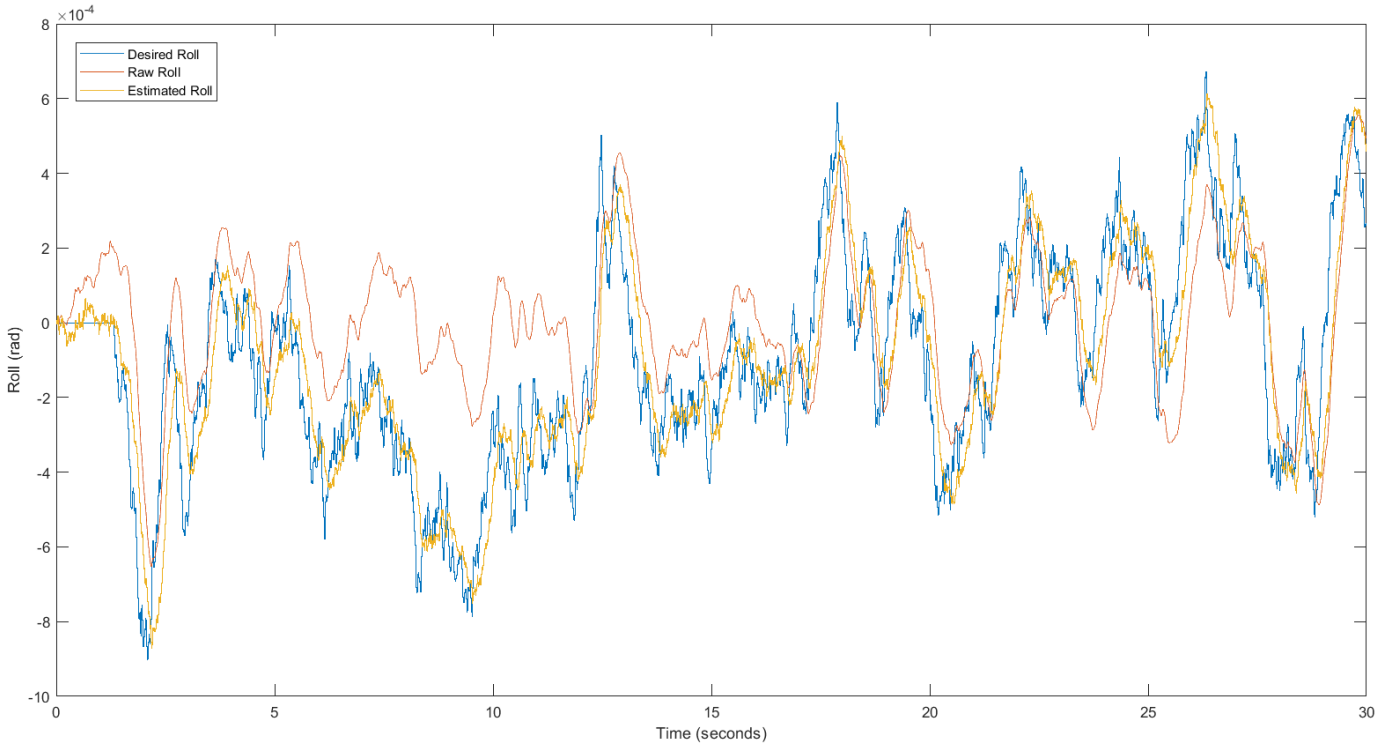

Figure A2: Roll data at hover

REFERENCES

1) Waslander, S.L., & Wang, C. (2009). Wind Disturbance Estimation and Rejection for Quadrotor Position Control.

2) S. J. Lee, S. Kim, K. H. Johansson and H. J. Kim, "Robust acceleration control of a hexarotor UAV with a disturbance observer," 2016 IEEE 55th Conference on Decision and Control (CDC), Las Vegas, NV, 2016, pp. 4166-4171, doi: 10.1109/CDC.2016.7798901.

3) Li Ding, Zhenwei Wang, "A Robust Control for an Aerial Robot Quadrotor under Wind Gusts", Journal of Robotics, vol. 2018, Article ID 5607362, 8 pages, 2018. https://doi.org/10.1155/2018/5607362

4) Dai, B., He, Y., Zhang, G. et al. Wind disturbance rejection for unmanned aerial vehicles using acceleration feedback enhanced H_∞ method. Auton Robot 44, 1271–1285 (2020). https://doi.org/10.1007/s10514-020-09935-8

5) Y. Guo, B. Jiang and Y. Zhang, "A novel robust attitude control for quadrotor aircraft subject to actuator faults and wind gusts," in IEEE/CAA Journal of Automatica Sinica, vol. 5, no. 1, pp. 292-300, Jan. 2018, doi: 10.1109/JAS.2017.7510679.

6) Manon Kok, Jeroen D. Hol and Thomas B. Schön (2017), "Using Inertial Sensors for Position and Orientation Estimation", Foundations and Trends® in Signal Processing: Vol. 11: No. 1-2, pp 1-153. http://dx.doi.org/10.1561/2000000094

7) Robot Dynamics Lecture Notes, Robotic Systems Lab, ETH Zurich HS 2017. https://ethz.ch/content/dam/ethz/special-interest/mavt/robotics-n-intelligent-systems/rsl-dam/documents/RobotDynamics2017/RD_HS2017script.pdf

8) Charles Tytler, Modeling Vehicle Dynamics – Quadcopter Equations of Motion, https://charlestytler.com/quadcopter-equations-motion/

9) D. Eberly, “Euler angle formulas,” Geometric Tools, LLC, Technical Report, 2008.

10) T. Luukkonen, Modelling and control of quadcopter, Independent research project in applied mathematics , Espoo: Aalto University, 2011.

11) Powers, Caitlin & Mellinger, Daniel & Kumar, Vijay. (2015). Quadrotor Kinematics and Dynamics. 10.1007/978-90-481-9707-1_71.

12) A. Gibiansky, Quadcopter Dynamics and Simulation, 2015, [online] Available:http://andrew.gibiansky.com/blog/physics/quadcopter-dynamics.

13) Robust control design for the trajectory tracking of a quadrotor - Scientific Figure on ResearchGate. Available from: https://www.researchgate.net/figure/The-quadrotor-model-body-and-earth-fixed-frame_fig1_328554518 [accessed 18 Dec, 2020]

14) Higgins, Chad & Froidevaux, Martin & Simeonov, Valentin & Vercauteren, Nikki & Barry, Caitlin & Parlange, Marc. (2012). The Effect of Scale on the Applicability of Taylor’s Frozen Turbulence Hypothesis in the Atmospheric Boundary Layer. Boundary-Layer Meteorology. 143. 10.1007/s10546-012-9701-1.

15) Digital simulation of atmospheric turbulence for Dryden and von Karman models T. R. Beal Journal of Guidance, Control, and Dynamics 1993 16:1, 132-138

16) Hakim, Teuku & Arifianto, Ony. (2018). Implementation of Dryden Continuous Turbulence Model into Simulink for LSA-02 Flight Test Simulation. Journal of Physics: Conference Series. 1005. 012017. 10.1088/1742-6596/1005/1/012017.

17) A. L. Salih, M. Moghavvemi, H. A. F. Mohamed and K. S. Gaeid, "Modelling and PID controller design for a quadrotor unmanned air vehicle," 2010 IEEE International Conference on Automation, Quality and Testing, Robotics (AQTR), Cluj-Napoca, 2010, pp. 1-5, doi: 10.1109/AQTR.2010.5520914.

18) Ngo, Ha Quang Thinh & Phuong, N.. (2018). A complete comparison to design complementary filter and kalman filter for aerial vehicle. International Journal of Mechanical Engineering and Technology. 9. 502-513.

19) Mohta, Kartik, "State Estimation, Control, And Planning For A Quadrotor Team" (2018). Publicly Accessible Penn Dissertations. 3360. https://repository.upenn.edu/edissertations/3360

20) Methods Comparison for the Attitude Determination of a Lightweight Buoy by Raw Data from IMU. Available from: https://www.researchgate.net/figure/implementation-of-the-complementary-filter-25_fig1_329119912 [accessed 18 Dec, 2020]

21) Ngo, Ha Quang Thinh & Phuong, N.. (2018). A complete comparison to design complementary filter and kalman filter for aerial vehicle. International Journal of Mechanical Engineering and Technology. 9. 502-513.

22) Tuning PID and FOPID Controllers using the Integral Time Absolute Error Criterion - Scientific Figure on ResearchGate. Available from: https://www.researchgate.net/figure/Generic-closed-loop-control-system-with-a-PID-controller_fig2_301866985 [accessed 18 Dec, 2020]

23) R. Mahony, T. Hamel and J. Pflimlin, "Nonlinear Complementary Filters on the Special Orthogonal Group," in IEEE Transactions on Automatic Control, vol. 53, no. 5, pp. 1203-1218, June 2008, doi: 10.1109/TAC.2008.923738.

24) Milam, Joshua Bruce, "Design and Evaluation of Novel Attitude Estimation System Using MEMS Sensors for Indoor UAS" (2018). Graduate Theses, Dissertations, and Problem Reports. 3711. https://researchrepository.wvu.edu/etd/3711